# Anomalies in the microwave power-dependent surface impedance of $YBa_2Cu_3O_{7-x}$ thin films

Anton V. Velichko,[1] Michael J. Lancaster,[1] Radoslav A. Chakalov,[2] and F. Wellhofer[2]
[1]*School of Electronics and Electrical Engineering, University of Birmingham, Birmingham, United Kingdom*
[2]*School of Physics and Astronomy, University of Birmingham, Birmingham, United Kingdom*
(Received 6 June 2001; published 1 March 2002)

Nonlinear microwave properties of two high-quality YBaCuO thin films on MgO substrate have been studied in zero and finite dc magnetic field (up to 12 mT) at 8 and 16 GHz using the coplanar resonator technique. Anomalous decrease in the surface impedance $Z_s = R_s + jX_s$ as a function of increasing microwave magnetic field $H_{rf}$ was found for both the samples. In one of the films anomalous behavior is only seen in $R_s(H_{rf})$ and only at low temperatures $T \leqslant 15$ K, whereas in the other one only $X_s(H_{rf})$ exhibits anomalies and mostly at intermediate $T$ (40–45 K). Impedance plane analysis in terms of $T$, frequency $f$, and $H_{rf}$ dependences of the $r$ parameter revealed that the anomalous behavior is most certainly governed by dynamics of quasiparticles, rather than vortices. At higher $H_{rf}$ ($\geqslant 10$ kA/m), however, a noticeable deviation from the quasiparticle scaling towards the vortex motion mechanisms was found. This indicates that in high microwave fields the anomalous affects in $Z_s(H_{rf})$ may be masked by or interfered with the vortex dynamics. Also some evidence is presented that the origin of the anomalies in $Z_s(H_{rf})$ is seemingly related to the oxygen content of the films.

DOI: 10.1103/PhysRevB.65.104522 PACS number(s): 74.25.Nf, 74.76.Bz, 74.25.Ha, 74.60.Ge

## I. INTRODUCTION

Nonlinear microwave properties of high-temperature superconductors (HTS's) cause a great deal of interest among the microwave HTS community in terms of both their significance for application and due to the rich and exciting physics involved (see, e.g., Refs. 1–3). From the classical theory and experiments on both low-temperature superconductors (LTS's) and HTS's it is known that superconducting properties usually deteriorate with elevated microwave $H_{rf}$ and dc $H_{dc}$ magnetic fields (see, e.g., Refs. 4–7). In terms of the surface impedance $Z_s = R_s + jX_s$, it means that both the surface resistance $R_s$ and the surface reactance $X_s$ increase with $H$ (here $H$ stands for both $H_{rf}$ and $H_{dc}$). Recently, however, a new extraordinary phenomenon in HTS thin films has been discovered: the anomalous decrease in $Z_s$ with a relatively weak (in a few mT region) $H_{rf}$ and $H_{dc}$.[8–11] Though similar anomalous effects has been reported in the past for LTS's subject to simultaneously applied ac and dc magnetic fields,[12,13] a closer look at the problem reveals that most of the classical concepts such as field-dependent surface barrier[13,14] and stimulated superconductivity[15] are unlikely to be responsible for the microwave anomalies discussed here.[10,16–18]

On the other hand, another two recently proposed mechanisms, namely the nonlinear grain shunted weak link model (GSWLM) (Ref. 18) and the modified two-fluid model (TFM) with the field-dependent quasiparticle scattering rate[19] are strong candidates for accounting for the aforementioned anomalies in $Z_s(H_{rf}, H_{dc})$. Both those models are capable of good description of experimental data on YBaCuO films, in which only $R_s$ decreases with $H$ ($H_{rf}$ or $H_{dc}$).[18,19] Here, in both the above mentioned scenarios $X_s(H)$ behaves in the normal way (i.e., rises). Recently, however, a number of new physical mechanisms were put forward that may give a consistent qualitative description of the correlated anomalies in both $R_s(H)$ and $X_s(H)$. Among those are the field-induced alignment of the magnetic impurity spins,[9,20] the opening of a superconducting subdominant *s*-wave-like energy gap,[21,22] the constructive quasiparticle interference at the grain-junction interface in a *d*-wave-like superconductor,[23] as well as other peculiar transport phenomena related to the spin-charge separation in quasi-one-dimensional systems,[24,25] intrinsic disorder,[26,27] the formation of stripes,[28] or novel quasi-particle concepts.[29] However, to the best of our knowledge, none of those concepts is yet embodied into a theoretical model for the surface impedance, which makes it impossible to compare the available experimental data with the theoretical predictions. Finally, there exists another explanation that the anomalous microwave effects attributed to HTS may actually be related to low temperature peculiarities in the loss tangent of MgO substrate.[30] However, the fact that microwave anomalies are seen in HTS films sputtered on other substrates[11,31] (such as $LaAlO_3$), as well as the fact that small dc magnetic fields can change the appearance of the anomalous effects dramatically[17] strongly suggest that there is a broad class of the microwave anomalies, which are most definitely related to superconductivity. In this paper we solely concentrate on latter category of the anomalies.

In what follows we present data on two high-quality (in terms of good low power $R_s$, $J_c$, $T_c$ and structural homogeneity) YBaCuO thin films and analyze those data in terms of temperature $T$, frequency $f$, and $H_{rf}$ dependences of the $r$ parameter ($r = \Delta R_s / \Delta X_s$). We show that a great variety of the available experimental data[9–11,16–19,31] is impossible to describe without attracting some sort of recovery effect in the Cooper pair density with increased magnetic field. We perform theoretical analysis of the data in terms of the differential loss tangent ($\tilde{r} = \partial R_s / \partial X_s$) within the TFM and modified Coffey-Clem model[32] (CCM). In the TFM the quasiparticle scattering is considered to be the dominant mechanism of microwave dissipation, whereas in the CCM the dissipation primarily originates in the vortex dynamics (including flux pinning, creep and flow). The analysis of our

 

TABLE I. Electrical and microstructural properties and growth parameters of the thin films.

| Sample | $T_c$, K | $J_c$, MA/cm$^2$ | $\Delta\omega$, ° | $c$ axis, Å | $T_{dep}$, °C | $R_s$, $\mu\Omega$ | $\lambda(0)$, nm |
|---|---|---|---|---|---|---|---|
| TF1 | 83 | 0.5 | 1.04 | 11.757 | 640 | 35 | 210 |
| TF2 | 88 | 2.2 | 0.55 | — [a] | 690 | 50 | 135 |

[a]The original data for this film are missing. In about 5 years after the film fabrication this parameter was measured to be 11.699, which corresponds to the oxygen content $\delta=6.78$.

data shows that the value of the $r$ parameter, as well as its $H$ and $f$ dependences fit best to a mechanism based on the quasiparticle scattering, rather than vortex nucleation and/or motion. In this respect, our conclusion is supported by recent observations of Rao *et al.*,[31] who found no hysteresis in the microwave losses in the anomalous regime, a strong indication of a dissipation mechanism not influenced by vortex dynamics.

The structure of the paper is as follows. In Sec. II the fabrication method, electrical and microstructural properties of the films studied in this work, as well as the measurement technique are described. Experimental results including $T$ and $H_{rf}$ dependences of the surface impedance $Z_s$ and $r$ parameter at two frequencies (8 and 16 GHz) and in various dc magnetic fields (up to 12 mT) are presented in Sec. III. Theoretical analysis in terms of $\tilde{r}$ within the TFM and CCM is described in Sec. IV. In Sec. V the experimental results are discussed and analyzed within the aforementioned two models, which is followed by conclusions in Sec. VI.

## II. SAMPLES AND MEASUREMENT TECHNIQUE

The two films studied here,[33] TF1 and TF2, are deposited by the *e*-beam coevaporation technique onto polished (001)-oriented MgO single crystal substrates $10\times10$ mm$^2$. The films are 350 nm thick. The *c*-axis misalignment of the films is typically less than 1%. The main electrical characteristics and microstructural properties, as well as the deposition conditions of the two films studied in this work are recapitulated in Table I. Here, the critical temperature $T_c$, the critical current density $J_c$ at 77 K , the rocking curve width $\Delta\omega$, the *c*-axis length, the film deposition temperature $T_{dep}$, the surface resistance $R_s$ at 12 K , and the zero-$T$ penetration depth $\lambda(0)$ for the two samples are given. The absolute values of $\lambda(0)$ were determined without resorting to any theoretical model by using the technique developed by Porch *et al.*[34] The method is based on measuring the microwave response of two coplanar resonators patterned on the same film. The two resonators have different ground plane-to-central strip spacing, but the same resonant frequency. This allows us to extract the absolute value of $\lambda$ at a fixed temperature $T_{min}$ by adjusting the guess value for $\lambda(T_{min})$ in order to make the temperature dependences of $\lambda$ for the two resonators coincide over the whole $T$ range. This method gives one a way of determining absolute values of $\lambda$ (with an accuracy of $\sim10\%$) without assuming a particular temperature variation, provided that the film is homogeneous over its area. The method also allows one to take into account the effect of finite film thickness. For more details see Ref. 34.

Preliminary measurements on the two films discussed here, TF1 and TF2, were presented in our earlier publication,[10] where they were designated as films TF2 and TF3, correspondingly. The data reported in the present paper were taken in about two year intervals after those reported in Ref. 10. Though the $H_{rf}$ dependences presented in these two papers cannot be directly compared since they were taken at different temperatures, the nonlinear behavior of the films is essentially the same. In particular, for film TF1 the anomalies are only seen at $T<20$ K and only in $R_s(H)$, whereas for TF2 the anomalies are observed at higher $T$ ($>40$ K) and are mostly seen in $X_s(H)$.

It should be noted here that when calculating the power dependences of $Z_s$ we made no correction for the change in the rf field distribution with increased $H_{rf}$ over the resonator area in the nonlinear regime. The importance of such correction has recently been highlighted by Reznik,[35] who demonstrated that a change in the field distribution with increased rf field amplitude may lead to a change in the power dependences of $Z_s$. However, the predictions of that model are only accurate in the case of strong nonlinearities [i.e., if $R_s(H)=R_0(1+bH^n)$, e.g., then $bH^n$ has to be $\gg1$], when exact analytical solutions for some of the model's equations exist. Fortunately, in our case relative increase in $R_s$ with the peak microwave field $H_{rf}$ is rather small (typically $\sim10\%$), or in other words $bH^n\ll1$, and therefore we think that the correction for the change in the rf field distribution should be negligible. In addition, even in the case of strong nonlinearities (see Figs. 3 and 4 in Ref. 35), the qualitative behavior of $Z_s(H)$ and other parameters (such as $b$, e.g.) does not change considerably when the correction is applied. Therefore, we believe that qualitative conclusions of our paper are not affected by the lack of the correction for the nonuniform $Z_s$ in the nonlinear regime. However, we also admit that in general case such corrections must be taken into account.

Approximately a year after all the main measurements reported here were completed, the reference part of film TF2 (Ref. 36) was x rayed to determine the oxygen content,[37] that proved to have deteriorated from $\gtrsim6.9$ to $\simeq6.78$ over the period specified above. As will be seen later, this change in the oxygen content strongly affected both the frequency dependence of the surface resistance $R_s$ of the film, as well as the appearance of the anomalous microwave effects which are the main subject of this paper.

## III. EXPERIMENTAL RESULTS

### A. $H_{rf}$ dependence of $Z_s$

Figure 1 demonstrates $H_{rf}$ dependences of $R_s$ and $X_s$ of sample TF1 taken at different $T$ (shown in the figure) at 8

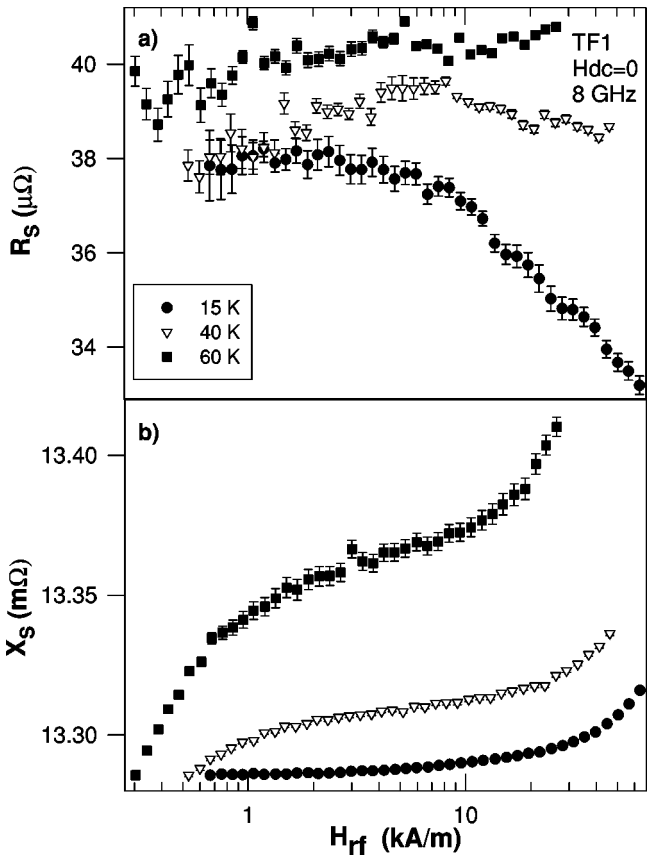


FIG. 1. $H_{rf}$ dependence of the surface resistance $R_s$ and the surface reactance $X_s$ for sample TF1 at various temperatures (given in the figure) and 8 GHz. The data at 40 and 60 K are offset along the vertical axis ($R_s$ is offset by 9.5 and 39 $\mu\Omega$, and $X_s$ is offset by 1.4 and 5.4 m$\Omega$ at 40 and 60 K, respectively) for clarity.

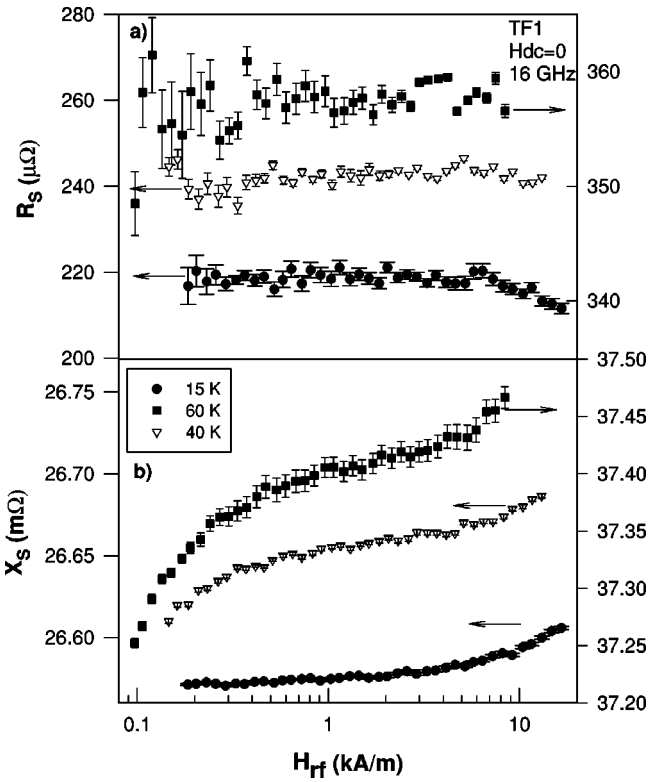


FIG. 2. $H_{rf}$ dependence of $R_s$ and $X_s$ for sample TF1 at various temperatures (given in the figure) and 16 GHz. The data at 40 K are offset along the vertical axis ($R_s$ is offset by 40 $\mu\Omega$, and $X_s$ is offset by 2.5 m$\Omega$) for clarity.

GHz. At 15 K an anomalous decrease in $R_s(H_{rf})$ accompanied by the conventional behavior (increase) of $X_s(H_{rf})$ is clearly seen, whereas at higher $T$ both $R_s(H_{rf})$ and $X_s(H_{rf})$ increase in the conventional way. The remarkable feature of this film is that functional behavior of $R_s(H_{rf})$ changes dramatically with $T$, whereas the shape of $X_s(H_{rf})$ remains virtually the same over the whole $T$ range. Here, the functional forms of $R_s(H_{rf})$ and $X_s(H_{rf})$ are generally not correlated (in sense that one of them may increase, while the other decreases).

$H_{rf}$ dependences of $R_s$ and $X_s$ of the same sample TF1 measured at 16 GHz and different $T$ are shown in Fig. 2. Both dependences are very similar to those at 8 GHz. The decrease in $R_s(H_{rf})$ is less pronounced at 16 GHz because of the narrower field range (due to lower quality factor of the resonator) at this frequency. The ''threshold'' field, i.e., the field above which $R_s(H_{rf})$ starts to fall seems to be nearly the same at both frequencies (see Figs. 1 and 2).

Figure 3 illustrates $H_{rf}$ dependences of $R_s$ and $X_s$ of sample TF2 measured at different $T$ and 8 GHz. The anomalous effects in this sample are more intricate than in TF1. At 15 K a shallow minimum in $R_s(H_{rf})$ is observed that is accompanied by perfectly ''normal'' behavior (i.e., increase) in $X_s(H_{rf})$. With increased $T$ (40 K), the anomaly in $R_s(H_{rf})$ gets washed out, whereas a profound anomaly (minimum) develops in $X_s(H_{rf})$ [see Fig. 3(b)]. Finally, at even higher $T$ (60 K) both $R_s(H_{rf})$ and $X_s(H_{rf})$ become nearly flat. As in the case of TF1, the qualitative behavior of $R_s(H_{rf})$ and $X_s(H_{rf})$ are generally not correlated. As far as 16 GHz data for this film are concerned [see Fig. 4], the overall behavior of $Z_s(H_{rf})$ is rather different from that seen at 8 GHz. Over the whole temperature range (15 to 60 K) neither $R_s(H_{rf})$ nor $X_s(H_{rf})$ exhibit any anomalies. In other words, they both increase as $H_{rf}$ rises. A possible reason for such dramatic difference of 8 and 16 GHz data may be a presence of local defects near the location of $H_{rf}$ maximum(s) for one of the resonant modes. Such defects could well mask or even suppress the anomalous effects. However, since no indication of such defects has been revealed by microstructural (AFM) measurements of the films, this scenario remains speculative.

### B. Influence of $H_{dc}$ on $Z_s(H_{rf})$

A dramatic effect of dc magnetic field (applied perpendicular to the film surface in the field-cooled regime) as small as a few mT on the power dependence of $Z_s$ of film TF1 at 15 K and 8 GHz is demonstrated in Fig. 5. The effect is especially pronounced in $X_s(H_{rf})$, for which $H_{dc}$ as low as 5 mT virtually inverts the functional form of $X_s(H_{rf})$ making it a ''mirror image'' of the zero-field curve (see Fig. 5). In addition, at all $H_{rf}$ in a finite $H_{dc}$ $X_s$ is lower than at zero field. In other words, the dc field seems to stimulate superconductivity reducing the penetration depth $\lambda$ and, hence,

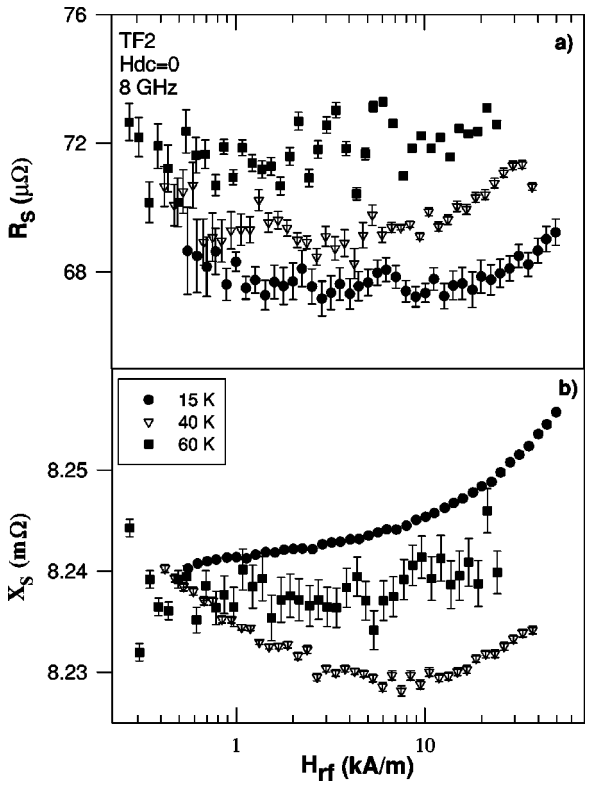


FIG. 3. $H_{rf}$ dependence of $R_s$ and $X_s$ for sample TF2 at various temperatures (given in the figure) and 8 GHz. The data at 40 and 60 K are offset along the vertical axis ($R_s$ is offset by 7.5 and 37 $\mu\Omega$, and $X_s$ is offset by 1.1 and 4.8 m$\Omega$ at 40 and 60 K, respectively) for clarity.

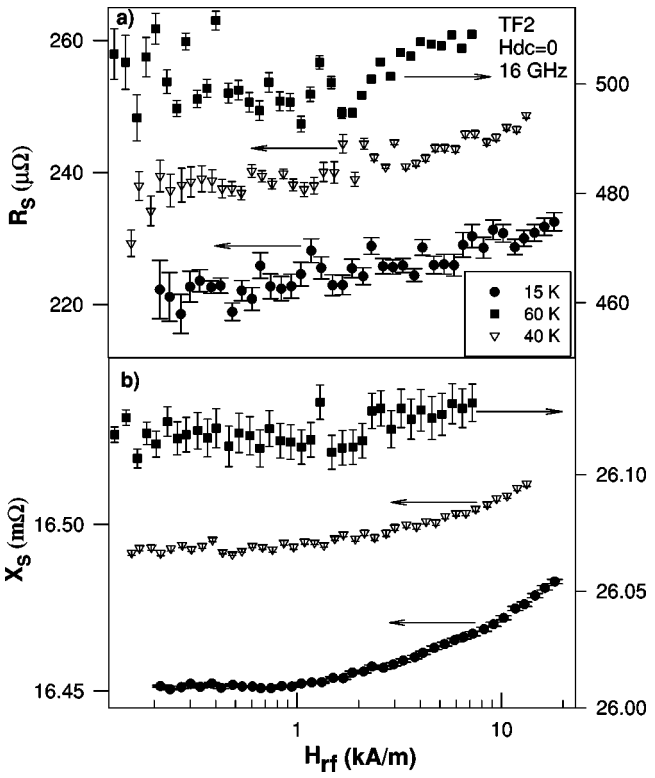


FIG. 4. $H_{rf}$ dependence of $R_s$ and $X_s$ for sample TF2 at various temperatures (given in the figure) and 16 GHz. The data at 40 K are offset along the vertical axis ($R_s$ is offset by 60 $\mu\Omega$, and $X_s$ is offset by 2.3 m$\Omega$) for clarity.

increasing the number of Cooper pairs. The effect of $H_{dc}$ on $R_s(H_{rf})$ is less noticeable and mainly consists in increasing the low power level of $R_s$ as well as slightly lowering the ''threshold'' field above which $R_s(H_{rf})$ decreases. Another feature to note is that all $R_s(H_{rf})$ curves measured at different $H_{dc}$ tend to merge with increased $H_{rf}$ ($\geqslant 10$ kA/m). Finally, at any given $H_{rf}$ both $R_s$ and $X_s$ are nonmonotonic functions of $H_{dc}$. At 16 GHz and 15 K $Z_s(H_{rf})$ curves (not shown in the figure) for film TF1 are quite similar to those measured at 8 GHz. Here again, enhanced $H_{dc}$ leads to lowering the threshold $H_{rf}$, above which the anomalous behavior comes into play.

At high temperatures (60 K) no anomalies in $R_s(H_{rf})$ are seen at either 8 GHz (see Fig. 6) or 16 GHz (not shown in the figure). The curves at 8 GHz are fairly flat up to some threshold field $H_{rf} \sim 10$–$20$ kA/m (depending on $H_{dc}$) and rise rapidly above that field. The threshold field is clearly reduced in the presence of the dc field, but the exact trend is not clear (e.g., the threshold field at 12 mT is higher than those at 5 and 10 mT, while those are lower than that at 0 mT, see Fig. 6). Generally, $R_s(H_{dc})$ is nonmonotonic within the whole range of $H_{rf}$. $X_s(H_{rf})$ has pretty much the same shape ($\sim H_{rf}^n$, where $n<1$ at low $H_{rf}$ and $n>1$ at higher $H_{rf}$) as it does at 15 K (see Figs. 1 and 2). $X_s(H_{dc})$ is generally monotonic within the whole range of $H_{rf}$ (except for $H_{rf} \leqslant 0.3$ kA/m and $H_{dc}$ of 5 mT at 8 GHz) with the main effect of $H_{dc}$ being diminishing $X_s$ (or $\lambda$) values. Above 10 mT a saturation of this ''recovery'' effect at 8 GHz is observed (data at 10 and 12 mT almost collapse onto a single curve, see Fig. 6). To summarize, we can say that unlike at low $T$ (15 K), at $T=60$ K $H_{rf}$ dependences of neither $R_s$ nor $X_s$ exhibit any anomalies, whereas $H_{dc}$ dependences do. Another common feature is that $R_s$ is generally increased with $H_{dc}$, though this dependence is nonmonotonic. At the same time, $H_{dc}$ always reduces $X_s$ and this dependence is monotonic.

$Z_s(H_{rf})$ for sample TF2 at 8 GHz, and 15 and 60 K and various dc fields are displayed in Figs. 7 and 8. The $R_s(H_{rf})$ curves at both $T$ are fairly flat up to $\sim 35$–$70$ kA/m ($\sim 44$–$88$ mT) at all $H_{dc}$ except 5 mT, at which $R_s(H_{rf})$ starts to rise at lower fields ($\sim 20$–$30$ kA/m). Unlike 15 K data, at 60 K 12 mT curve also exhibits a rise in $R_s$ above $\sim 10$ kA/m. No anomalies are seen in $R_s(H_{rf})$ at any of the dc fields. $H_{dc}$ dependence of $R_s$ is again nonmonotonic at all $H_{rf}$, as it is for film TF1, with the in-field $R_s$ values increased compared with the zero field ones. The most pronounced increase in $R_s$ at both $T$ is caused by $H_{dc}=5$ mT, whereas higher $H_{dc}$ tends to bring the $R_s(H_{rf})$ curves down close to the zero-field dependence. The shape of $R_s(H_{rf})$ curves is generally unaffected by $H_{dc}$ except 5 mT (and 12 mT at 60 K) data. At the same time, the shape of $X_s(H_{rf})$ is noticeably affected by $H_{dc}$. For instance, at 15 K $H_{dc}$ of 10 and 12 mT are seen to produce a shallow minimum at intermediate values of $H_{rf}$ ($\sim 7$–$15$ kA/m). At 60 K similar effect is observed at 5 mT with the minimum being at lower $H_{rf}$ ($\sim 4$–$5$ kA/m). Here, at both temperatures $H_{dc}$ of 5 mT

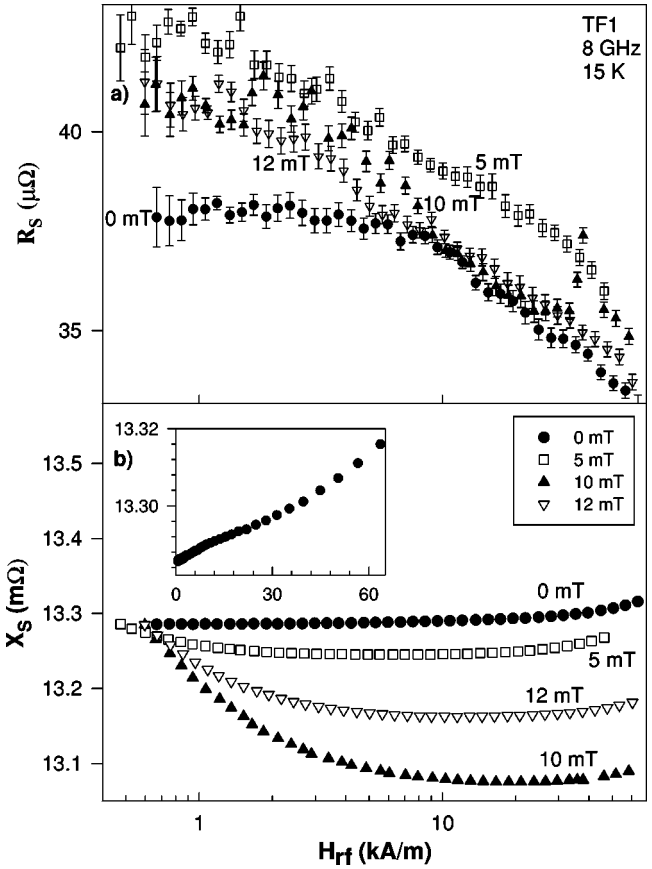


FIG. 5. $H_{rf}$ dependence of $R_s$ and $X_s$ for sample TF1 in various dc magnetic fields $H_{dc}$ (shown in the figure) at 15 K and 8 GHz. The inset in the lower figure demonstrates $X_s(H_{rf})$ at 0 mT on an expanded scale.

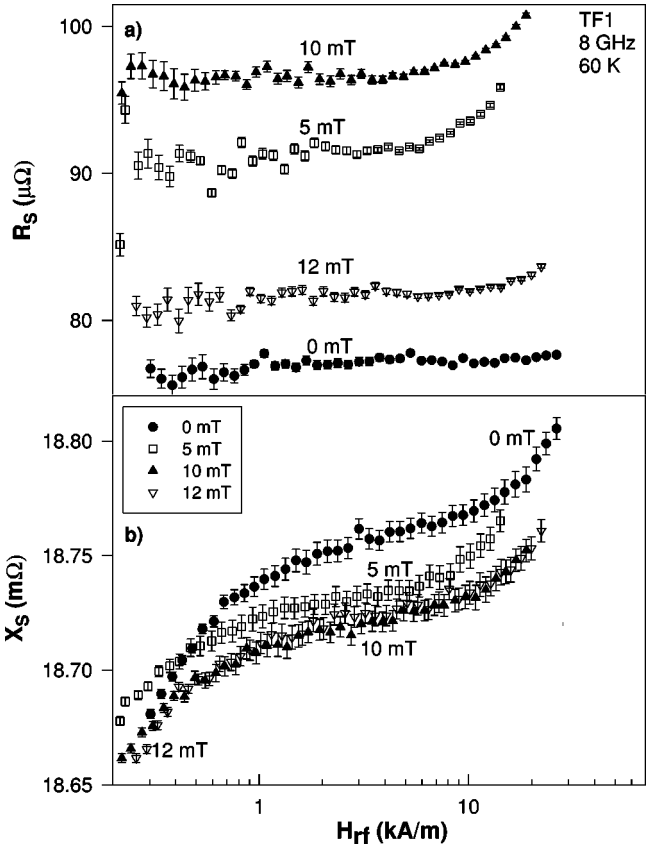


FIG. 6. $H_{rf}$ dependence of $R_s$ and $X_s$ for sample TF1 in various dc magnetic fields $H_{dc}$ (shown in the figure) at 60 K and 8 GHz.

evokes a very rapid growth of $X_s(H_{rf})$ at $H_{rf} \geqslant 20$ kA/m [similarly to its effect on $R_s(H_{rf})$]. Thus, similarly to film TF1, certain values of $H_{dc}$ are seen to greatly affect the shape of $X_s(H_{rf})$, without having much of an effect on the shape of $R_s(H_{rf})$. Here, the main effect of $H_{dc}$ is a nonmonotonic increase in $R_s$ at all values of $H_{rf}$ and a nonmonotonic behavior in $X_s(H_{rf})$.

### C. Frequency dependence of $R_s$ in both linear and nonlinear regimes

The temperature dependence of $R_s$ for both samples, TF1 and TF2, at both resonance modes (8 and 16 GHz) and at two values of $H_{rf}$ (1 and 7 kA/m) are shown in Figs. 9(a),9(b). The data at 8 GHz are scaled up to 16 GHz using the conventional formulas $R_s \sim f^n$, where $n$ is expected to be $\sim 2$. For both films the data collapse well onto a single curve at low $T$ (below 50 and 40 K for TF1 and TF2, respectively). At higher $T$ there is a noticeable discrepancy between the 8 and 16 GHz curves that might be caused by presence of local inhomogeneities at the location of $H_{rf}$ maximum for one of the resonant modes, as was mentioned earlier. However, having no microstructural evidence of existence of such defects in the film, we admit that the change in the frequency scaling with $T$ remains unexplained.

There are two important observations that follow from Figs. 9(a),9(b). First, the frequency scaling of $R_s$ for both the films is different from the conventional $f^2$ scaling expected for homogeneous superconductor ($n = 2.54$ and 1.73 for TF1 and TF2, respectively); and second, the frequency scaling remains unchanged in both low (1 kA/m) and high (7 kA/m) $H_{rf}$ ranges. At first glance, the difference in the $H_{rf}$ values may seem to be not that significant to justify the conclusion that the frequency scaling is the same for both the linear and nonlinear regimes. However, later on it will be shown that the same scaling holds within much broader $H_{rf}$ range (from 0.5 to 20 kA/m). The first fact ($n \neq 2$) implies that local defects may be responsible for the non-$\omega^2$ scaling [see, e.g., Ref. 2]. The other fact seems to imply that the dissipation mechanism at high microwave powers (nonlinear regime) is the same as that at low $H_{rf}$ (linear regime), and is therefore, most likely dominated by quasiparticle scattering rather than vortex motion. This preliminary conclusion will be further supported by comprehensive impedance plane analysis performed in the later sections of the paper.

Frequency scaling of $R_s$ for sample TF1 when field cooled in both low (1 kA/m) and high (7 kA/m) $H_{rf}$ ranges was found to be essentially the same (within an accuracy of 5%, not shown in the figure). However, in a finite dc field the scaling breaks at slightly lower (by about 5–10 K) $T$. Admitting the concept of local defects it is quite reasonable to expect that trapped magnetic flux should weaken superconductivity in the intergrain boundaries (or defects) and make

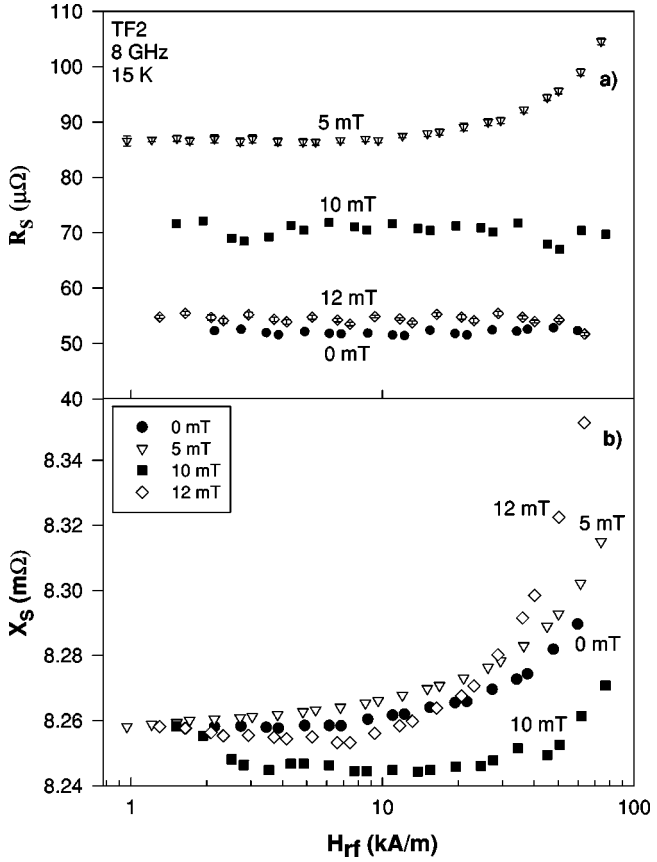


FIG. 7. $H_{rf}$ dependence of $R_s$ and $X_s$ for sample TF2 in various dc magnetic fields $H_{dc}$ (shown in the figure) at 15 K and 8 GHz.

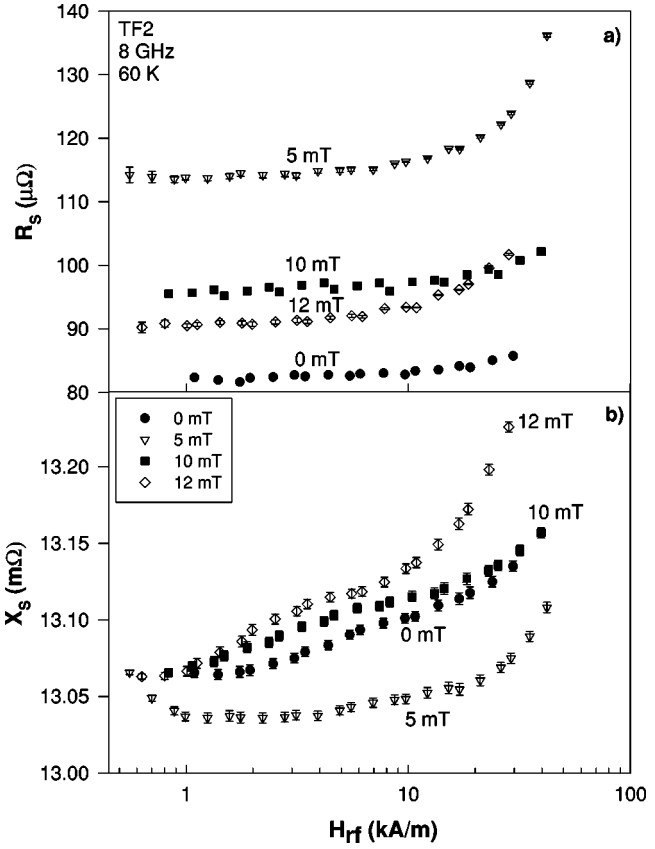


FIG. 8. $H_{rf}$ dependence of $R_s$ and $X_s$ for sample TF2 in various dc magnetic fields $H_{dc}$ (shown in the figure) at 60 K and 8 GHz.

them come into play at lower $T$. Again, we see that even with a trapped magnetic flux the same frequency scaling holds for both low and high microwave power regimes. Therefore, though vortices are inevitably present in the sample upon the field cooling, they do not seem to dominate the microwave dissipation in either of those cases.

Figures 10(a),10(b) demonstrate $R_s(H_{rf})$ curves measured at both modes (8 and 16 GHz) at various $T$ (shown in the figure) for samples TF1 and TF2, respectively. The curves at 8 GHz were scaled up to 16 GHz using the same frequency exponent $n$ ($R_s \sim f^n$) over the entire $H_{rf}$ range. Two remarkable features have to be noted here. For film TF1 the scaling exponent in the anomalous regime ($T=15$ K,$n=2.5$) is higher that in the normal regime ($T=60$ K, $n=2.2$). Similarly, for sample TF2 at 40–45 K where the most profound anomalies in $X_s(H_{rf})$ are seen, the scaling exponent is higher, $n \simeq 1.9$, than the corresponding value at low temperatures $n=1.7$ ($T=15$ K), where no legible anomalies are seen in $X_s(H_{rf})$, and a very shallow minimum is seen in $R_s(H_{rf})$. Nearly the same scaling exponent ($\simeq 1.9$) holds for TF2 at higher $T$ (up to 60 K, not shown in the figure). Here again, we can see that the same frequency scaling holds for both low ($H_{rf} \geqslant 0.5$ kA/m) and high ($H_{rf} \leqslant 20$ kA/m) microwave power regimes thus supporting our conclusion that the dissipation mechanisms in linear and nonlinear regimes of the films studied here appears to have a similar nature.

Temperature dependences of $R_s$ at 8 and 16 GHz at low microwave power ($-10$ dBm,$H_{rf} \simeq 0.3$ kA/m) are shown in Figs. 11(a),11(b) for samples TF1 and TF2, respectively. The data at 8 GHz are scaled up to 16 GHz. As one can see from Fig. 11(a), frequency scaling for TF1 changes significantly with $T$. In the lower $T$ range ($T \leqslant 20$ K), the scaling exponent $n \simeq 2.5$, then it reduces to $\simeq 2.3$ at 20–35 K, and finally reduces to $\simeq 2.06$ above 40 K. This again demonstrates that the conventional frequency scaling ($n \simeq 2$) for TF1 holds only in high-$T$ range ($T \geqslant 40$ K), whereas at low $T$, where the anomalies in $R_s(H_{rf})$ are observed, the scaling factor is enhanced by approximately 25%.

Figure 11(b) illustrates frequency scaling for TF2 deduced from the measurements which were taken some year after the initially presented measurements on that sample had been made (and in about 5 years after the film fabrication). The scaling exponent in these later measurements is very close to 2 ($n \simeq 2.02$) within the whole $T$ range. In addition, no anomalies in either $R_s(H_{rf})$ or $X_s(H_{rf})$ were seen in sample TF2 after that period. According to the x-ray analysis, the oxygen content of TF2 has been significantly reduced ($\delta \simeq 6.78$) as compared to that ($\delta \geqslant 6.9$) of the "just fabricated" film. This gives us a hint that origin of the anomalies is strongly related to the oxygen content of the HTS films. An active research in this field is currently being carried out by Hein *et al.*,[38] who are studying the effect of oxygen content on the appearance of the microwave anomalies in the nonlinear surface impedance of YBaCuO films on MgO. How-

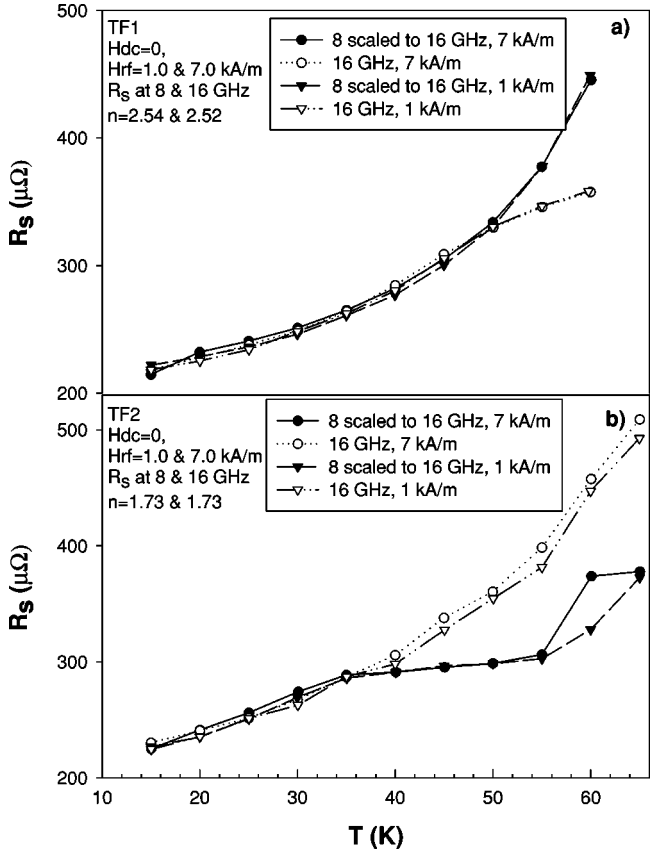


FIG. 9. Temperature $T$ dependence of $R_s$ for samples (a) TF1 and (b) TF2 at 8 and 16 GHz measured at two values of $H_{\rm rf}$ (1 and 7 kA/m) in zero dc field. Data at 8 GHz are scaled up to 16 GHz using the conventional relationship $R_s \sim f^n$. Scaling exponents obtained via the least square fitting of 8 GHz to 16 GHz data are given in the figure.

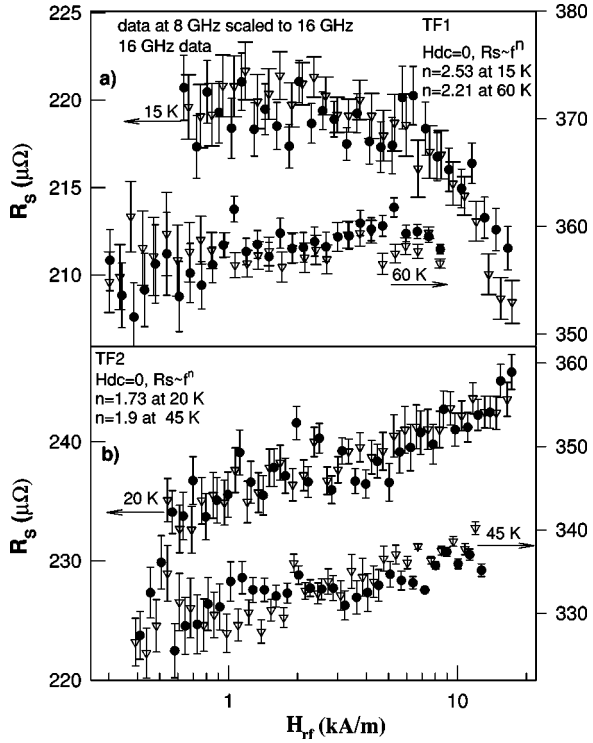


FIG. 10. $H_{\rm rf}$ dependences of $R_s$ for samples (a) TF1 and (b) TF2 at 8 GHz (open symbols) and 16 GHz (filled symbols) measured at two different temperatures (15 and 60 K and 20 and 45 K, for samples TF1 and TF2, respectively) and zero dc field. Data at 8 GHz are scaled up to 16 GHz using the conventional relationship $R_s \sim f^n$. Scaling exponents obtained via the least square fitting of 8 GHz to 16 GHz data are given in the figure.

ever, this issue is investigated rather scarcely so far, and no accurate understanding of this effect yet exists.

### D. *r* parameter analysis: Temperature, frequency, dc, and rf magnetic field dependences

The way we define temperature, frequency and dc field dependences of the $r$ parameter in this section is as follows:

$$r(A) = \frac{[R_s(H_{\rm rf}) - R_s(H_{\rm rf}^{\rm min})]_A}{[X_s(H_{\rm rf}) - X_s(H_{\rm rf}^{\rm min})]_A}, \tag{1}$$

where $A$ represents either $T$, or $f$ or $H_{\rm dc}$, with the other two parameters being held constant. Here, $H_{\rm rf}$ dependence of $r$ is defined simply as

$$r(H_{\rm rf}) = \frac{[R_s(H_{\rm rf}) - R_s(H_{\rm rf}^{\rm min})]}{[X_s(H_{\rm rf}) - X_s(H_{\rm rf}^{\rm min})]}.$$

#### *1. Temperature and frequency dependences of r parameter*

Temperature dependences of the $r$ parameter for film TF1 at 8 and 16 GHz and various values of $H_{\rm rf}$ are shown in Figs. 12(a) and 12(b). As one can see, the $r(T)$ curves deviate from each other at low temperatures ($T \geqslant 20$ K) and tend to collapse with increased $T$. In this low-$T$ range both $H_{\rm rf}$ and $f$ dependences of the $r$ parameter are clearly noticeable. Generally, the $r$ parameter increases with $T$ at low temperatures, then passes through a maximum around $T \sim 25$ K, and slowly decreases with further increase in $T$. However, $H_{\rm rf} = 2$ kA/m data clearly fall out of this common trend showing a consistent decrease of $r$ with $T$. Also, we can see that $r$ clearly increases with frequency in the low-$T$ range where the nonlinear anomalies in $Z_s(H_{\rm rf})$ occur, and is nearly frequency independent at higher $T$.

Temperature dependences of the $r$ parameter for film TF2 at 8 and 16 GHz and various values of $H_{\rm rf}$ are shown in Figs. 13(a) and 13(b). Similarly to TF1, for this sample the $r$ parameter noticeably increases with frequency in the temperature range where the microwave anomalies take place (between 40 and 50 K), whereas it is virtually frequency independent at other $T$. Contrary to sample TF1, though, the temperature dependence of $r$ for TF2 is fairly flat over the whole $T$ range except a sharp maximum at 16 GHz that is seen in the anomalous range ($40 < T < 50$ K). However, it is worth remembering that at 16 GHz no impedance anomalies are observed for this sample and, therefore, this maximum in $r(T)$ should not be attributed to the mechanism of the anomalies.

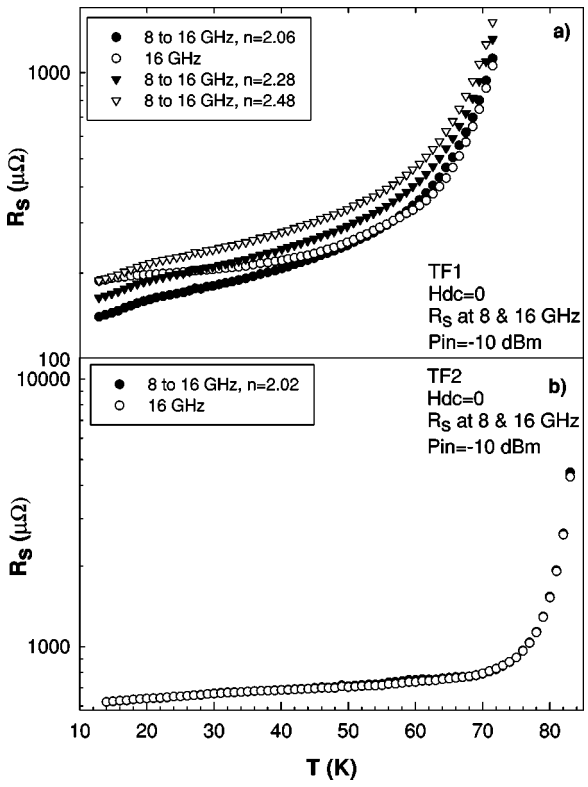


FIG. 11. $T$ dependence of $R_s$ for samples (a) TF1 and (b) TF2 (taken some year after all other measurements discussed earlier in the text were made) at 8 and 16 GHz measured at low microwave power $P_{rf}=-10$ dBm and zero dc field. Data at 8 GHz are scaled up to 16 GHz using the conventional relationship $R_s \sim f^n$. Scaling exponents obtained via the least square fitting of 8 to 16 GHz data are given in the figure.

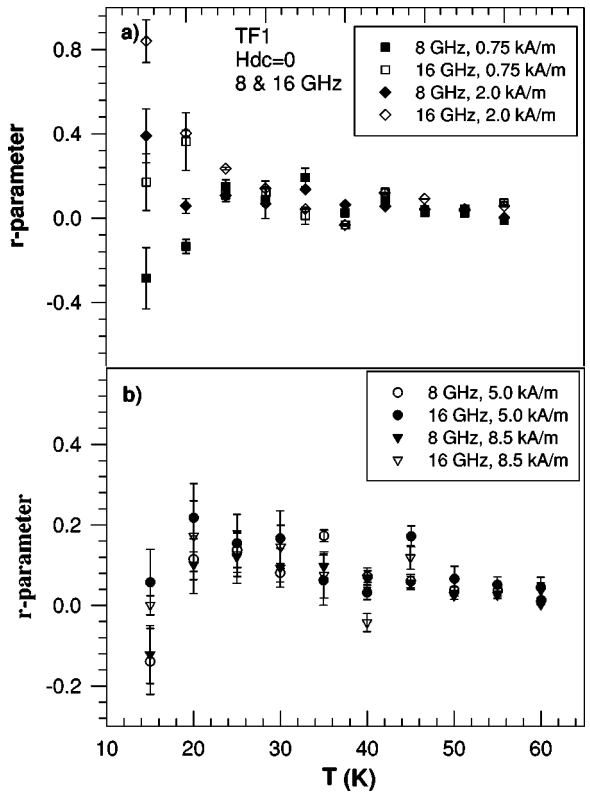


FIG. 12. $T$ dependence of the $r$ parameter for sample TF1 at 8 (filled symbols) and 16 GHz (open symbols) measured at various values of $H_{rf}$ (given in the figure) and zero dc field.

#### *2. dc and rf magnetic field dependences of r parameter*

$H_{rf}$ dependences of the $r$ parameter at 8 GHz, 15 K and various values of $H_{dc}$ for samples TF1 and TF2 are shown in Figs. 14(a) and 14(b), respectively. For TF1 at $H_{rf} \geqslant 3$ kA/m the dc field significantly affects the $r(H_{rf})$ curves making them nearly collapse for $H_{dc} \geqslant 10$ mT. As one can see, $H_{dc}$ also remarkably reduces values of $r$ at high $H_{rf}$. Another prominent feature is that at zero $H_{dc}$ $r$ values are negative for certain range of $H_{rf}$, whereas for the in-field data $r$ values are always positive. Thus, the abrupt change in the values, sign and $H_{rf}$ dependences of the $r$ parameter with dc field indicate that the frozen magnetic flux seems to change the mechanism of the nonlinear response for this sample. Furthermore, since in both zero and finite dc fields we observe anomalous power dependences of either $R_s$ or/and $X_s$, we can conclude that there must exist different mechanisms for the nonlinear microwave anomalies. In particular, in the cases of uncorrelated [either $R_s(H_{rf})$ or $X_s(H_{rf})$ decreases] and correlated [both $R_s(H_{rf})$ or $X_s(H_{rf})$ decrease simultaneously] behaviors the anomalous mechanisms appear to be different (according to different values, sign and field dependences of the $r$ parameter). For film TF2 [see Fig. 14(b)] $H_{dc}$ changes noticeably neither $r(H_{rf})$ nor $r$ values, except for the 5 mT curve, for which $H_{dc}$ leads to visible increase in $r$ with $H_{rf}$ above $\sim 10$ kA/m. Thus it can be concluded that for TF2 the presence of frozen dc flux does not generally change the mechanism of nonlinearity. The case of 5 mT is, however, an exception which suggests that at high $H_{rf}$ ($\geqslant 10$ kA/m) this particular dc field may cause a change in the dissipation mechanism.

$r(H_{rf})$ at 8 GHz, 60 K and various values of $H_{dc}$ for samples TF1 and TF2 are shown in Figs. 15(a) and 15(b), respectively. For TF1, similarly to 15 K data, a noticeable effect of the dc field upon $r(H_{rf})$ is clearly seen for $H_{rf} \geqslant 10$ kA/m. Contrary to the low $T$ results, however, at 60 K $H_{dc}$ has an absolutely opposite effect on both $r(H_{rf})$ and $r$ values, i.e., it enhances $H_{rf}$ dependences and increases $r$ values [cf., Figs. 14(a) and 15(a)]. This, again, suggests that for TF1, similar to low-$T$ data, in the high-power regime the mechanism of dissipation in zero $H_{dc}$ appears to be different from that in a finite dc field. However, the dissimilarity in this case is qualitatively different as compared to the one at 15 K. For film TF2 at 60 K, similarly to the data at 15 K [cf., Figs. 14(b) and 15(b)], $H_{dc}$ does not generally lead to any apparent changes in either the functional form of $r(H_{rf})$ or $r$ values. As with the 15 K data, at 60 K the 5 mT curve clearly falls out of the general trend. This curve clearly deviates from the rest of the data for $H_{rf} \geqslant 3$ kA/m, which qualitatively correlates with the anomalous decrease seen in $X_s(H_{rf})$ at 5 mT and 60 K (see Figs. 8). Here, $r$ values turn negative with increased $H_{rf}$ because of the noncorrelated behavior of $R_s(H_{rf})$ and $X_s(H_{rf})$ at this temperature.

In Fig. 16 $H_{rf}$ dependences of the $r$ parameter for film TF1 at 8 and 16 GHz, 15 K and various dc fields are pre-

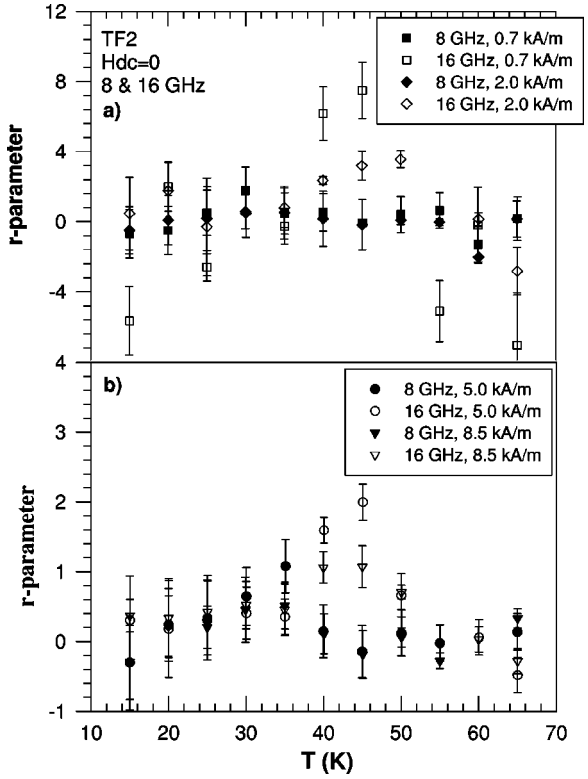


FIG. 13. $T$ dependence of the $r$ parameter for sample TF2 at 8 (filled symbols) and 16 GHz (open symbols) measured at various values of $H_{\rm rf}$ (given in the figure) and zero dc field.

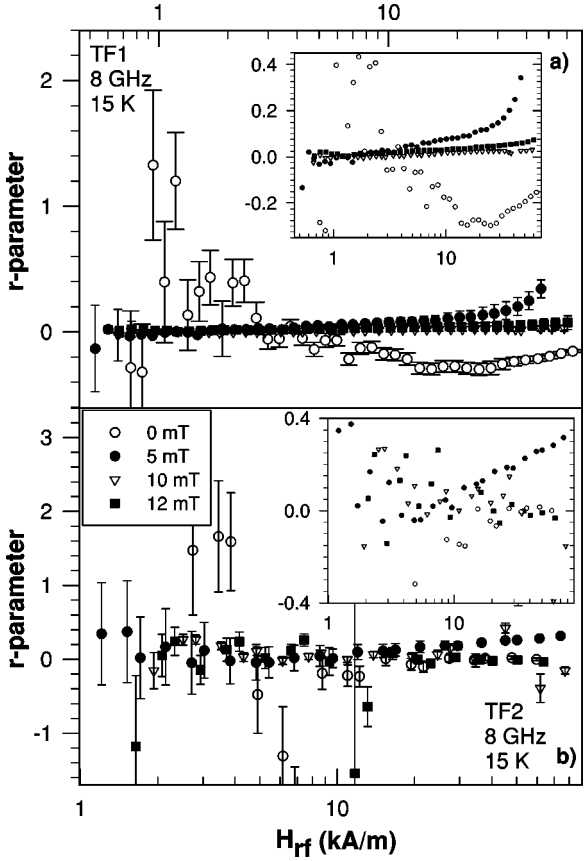


FIG. 14. $H_{\rm rf}$ dependence of the $r$ parameter for samples (a) TF1 and (b) TF2 at 8 GHz, measured at various values of $H_{\rm dc}$ (given in the figure) and 15 K. The insets demonstrate the data on an expanded scale.

sented. Two important features have to be noted here. First, at 0 mT $r$ parameter is virtually frequency independent. However, a noticeable frequency dependence of the $r$ parameter develops and become stronger with increased $H_{\rm dc}$. Second, the general trend of $r(H_{\rm rf})$ also changes from decreasing at $H_{\rm dc}=0$ to increasing one with enhanced $H_{\rm dc}$.

## IV. THEORETICAL ANALYSIS

To get a deeper insight into the mechanisms responsible for the normal and anomalous nonlinear behavior of our films, we have performed the impedance plane analysis of the experimental data within the framework of two theoretical models, TFM [see, e.g., Ref. 2] and modified CCM.[32] In the classical TFM the surface impedance can be presented in terms of the conductivity ratio, $y=\sigma_1/\sigma_2$, as was formulated by Hein *et al.*[2,9]

$$Z_s=R_s-jX_s=R_c[\varphi_-(y)-j\varphi_+(y)], \tag{2}$$

where $R_c=\sqrt{(\omega\mu_0)/2\sigma_1}$ is the classical surface resistance, and the scaling functions, $\varphi_\pm(y)$ are given by

$$\varphi_\pm(y)=\sqrt{\frac{y}{1+y^2}[\sqrt{(1+y^2)}\pm 1]}. \tag{3}$$

Here, the relationship between the differential loss tangent $\tilde{r}$ and $y$ reads

$$\tilde{r}=\frac{\partial R_s}{\partial X_s}=\frac{y}{\sqrt{1+y^2}-1}\frac{[(Ky^2+K-1)(\sqrt{1+y^2}-1)-y^2]}{[(Ky^2+K-1)(\sqrt{1+y^2}+1)+y^2]}, \tag{4}$$

where

$$y=y(K)=\phi\frac{(1-K)}{K} \tag{5}$$

and

$$K=K(h)=\frac{1}{1+\phi^2}[x_{s0}^2(1-h^2)^2+\phi^2]. \tag{6}$$

Here $K$ is a function that encompasses dependence of the complex conductivity $\sigma=\sigma_1+j\sigma_2$ (and, hence, that of $Z_s$) on various external parameters (such as $T$, $H$, $f$, etc.) via dependence of the superconducting carrier concentration, $x_s$ on those parameters. The meaning of various parameters in the above equations is as follows: $\phi=\omega\tau$ with $\omega$ and $\tau$ being the operating angular frequency and the quasiparticle scattering time, respectively; $x_{s0}=2n_{s0}/n_t$ with $n_{s0}$ and $n_t$ being the low field concentration of Cooper pairs and the total electron concentration, respectively; $h=H/H_c$, where $H_c$ is the scaling field close in magnitude to the thermodynamical critical field.

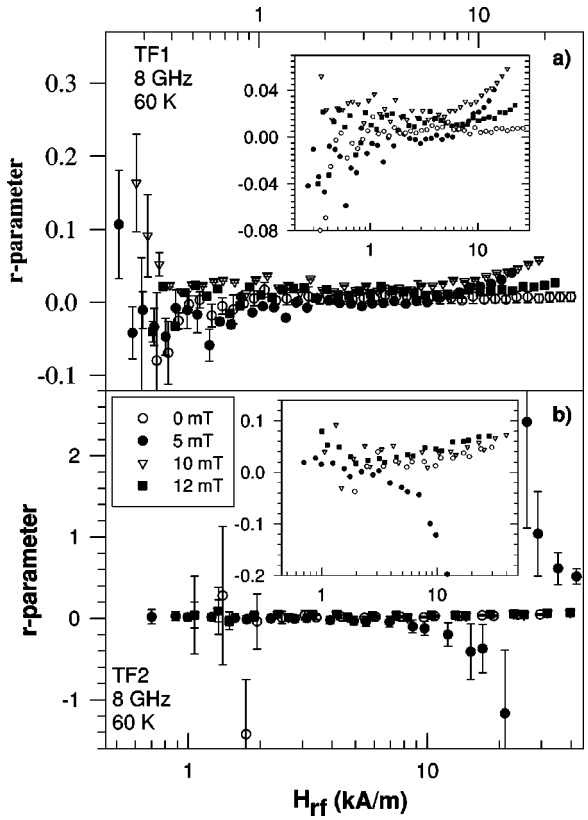


FIG. 15. $H_{\rm rf}$ dependence of the $r$ parameter for samples (a) TF1 and (b) TF2 at 8 GHz, measured at various values of $H_{\rm dc}$ (given in the figure) and 60 K. The insets demonstrate the data on an expanded scale.

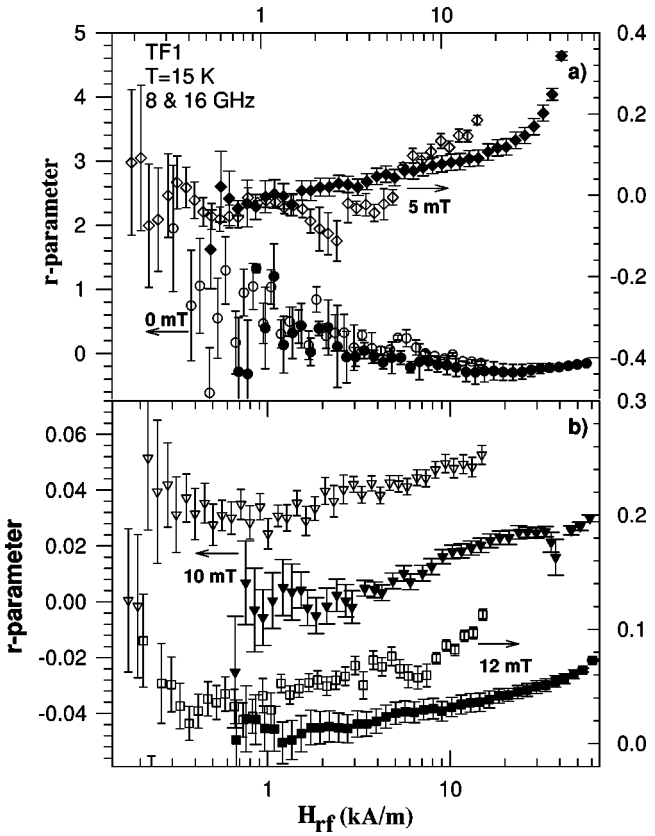


FIG. 16. $H_{\rm rf}$ dependence of the $r$ parameter for sample TF1 at 8 (filled symbols) and 16 (open symbols) GHz, measured at various values of $H_{\rm dc}$ (given in the figure) and 15 K.

The exact dependences of $\sigma_1$ and $\sigma_2$ on $K$ are given by[6]

$$\sigma_1=\omega\mu_0(1-K),$$

$$\sigma_2=\frac{\omega\mu_0}{K}. \tag{7}$$

The exact procedure of the data analysis in terms of $\tilde{r}$ within the TFM is described in Ref. 9. Briefly, from the experimental values of $\tilde{r}$ one can deduce the corresponding $y$ values using Eq. (4), and then $\varphi_{\pm}$ values can be found using Eq. (3). The next step is to deduce $R_c$ values using Eq. (2), experimentally measured $\Delta R_s=R_s(H_{\rm rf})-R_s(0)$ and $\Delta X_s=X_s(H_{\rm rf})-X_s(0)$, and $\varphi_{\pm}$ found from Eq. (3). Here, the $R_c$ values deduced from $\Delta R_s$ and $\Delta X_s$ should ideally be the same, which is another check of consistency of the TFM scaling.

We should note here that standard TFM is a linear model. We introduce the nonlinearity into the standard TFM by incorporating the field-dependent carrier concentration $x_s$ into the expression for the function $K(H)$ [Eq. (6)]. We believe this is a well justified assumption to make since even in the Meissner state the nonlinearity does arise due to Ginzburg-Landau depairing or nonlinear pair breaking mechanism, which predicts that $x_s\sim H_{\rm rf}^2$. Similar assumptions have been made by other authors when considering the nonlinearity within the weakly coupled grain models.[5,18,39]

The other model we used for the analysis of our data is the Coffey-Clem model for the rf surface impedance in the presence of vortex motion.[32] According to Coffey and Clem,[32] the surface impedance in the most general case can be written in terms of the complex penetration depth, $\tilde{\lambda}$ as follows:

$$Z_s=R_s-jX_s=-j\omega\mu_0\tilde{\lambda}, \tag{8}$$

where $\tilde{\lambda}$ is expressed as

$$\tilde{\lambda}=\left(\frac{\lambda_L^2+j\delta_{vc}^2/2}{1-2j\lambda_L^2/\delta_{\rm nf}^2}\right)^{1/2}, \tag{9}$$

where $\lambda_L$ is the London penetration depth, $\delta_{vc}$ is the complex vortex penetration depth (that takes into account the effects of flux pinning, creep, and flow), and $\delta_{\rm nf}$ is the normal fluid penetration depth. The field, temperature, and frequency dependences for all those quantities can be found in Ref. 32 and will not be reproduced here. There is also some indication in the literature that the pinning constant $\kappa_p$ (and, hence, the pinning frequency, $\omega_p=\kappa_p/\eta$) may be field dependent.[40,41] To account for this, we considered $\kappa_p$ to be field dependent in the following form:

$$\kappa_p=\kappa_{p0}\frac{(1-t^2)^{3/2}}{1+B/B_J}, \tag{10}$$

where the field dependence of $\kappa_p$ is essentially determined by that of the critical current density $J_c$. For an inhomogeneous superconductor containing weak links the field dependence of $J_c$ is well described by the following empirical relationship:[7]

$$J_c = \frac{J_{c0}}{1 + B/B_J}, \tag{11}$$

where the scaling field

$$B_J = \frac{\Phi_0}{2a\lambda_L}$$

or

$$B_J = \frac{\Phi_0}{2\lambda_J \lambda_L},$$

depending on whether the weak links are short or long Josephson Junction like, respectively.

We have to note here that CCM is a linear model and generally not applicable to the nonlinear regime. However, for the present analysis we adopted a quasi-static approximation, i.e., we assumed similarity in the effect of dc and rf fields on the microwave properties. Such a similarity might be possible since the characteristic frequencies of vortex nucleation and depinning for epitaxial YBaCuO films can be of order 100 GHz (see, e.g., Ref. 7), which is much higher than the operating frequency of our measurements. Of course, this does not guarantee that the quasi-static approximation may be rigorously justified, just because, e.g., dc and rf fields may penetrate differently into the sample. However, taking into account the difference between the effect of dc and rf fields on $Z_s$ would unlikely change our conclusions about the values of the $r$ parameter, which for all vortex motion mechanisms (both in linear and nonlinear regimes) are known to be of order unity.[7]

The results of the theoretical simulation within both TFM and CCM together with the most representative experimental data are shown in Fig. 17. The parameters used for the simulation such as zero temperature penetration depth $\lambda_L(0)$, upper critical field $B_{c2}(0)$, residual normal fluid resistivity $\rho_n(0)$, the barrier height of the periodic pinning potential $U_0$, vortex viscosity $\eta$, low field pinning constant $\kappa_{p0}$ are given in the caption to Fig. 17. The difference between various TFM curves correspond to different values of $R_s(0)$ and $X_s(0)$ [which in turn correspond to different values of $\varphi_{\pm}(0)$] for different samples and experimental conditions (specified in the figure).

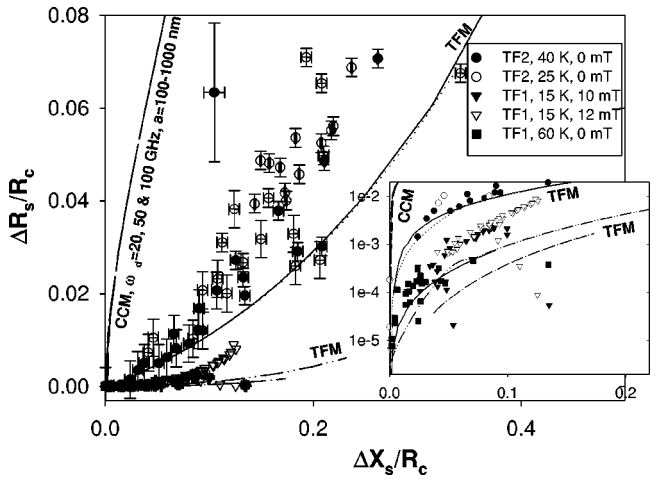


FIG. 17. Change in the surface resistance $\Delta R_s$, versus change in the surface reactance $\Delta X_s$, normalized by the classical surface resistance $R_c$ for samples TF1 and TF2 at various $T$ and $H_{\rm dc}$ (given in the figure). Theoretical curves simulated within the TFM and modified CCM are presented by lines (labeled in the figure). The inset shows the data on an expanded scale and logarithmic scale in $\Delta R_s/R_c$. The parameter involved in the simulation are as follows: $\lambda(0) = 140$ nm, $B_{c2}(0) = 112$ T, $\rho_n(0) = 2\times10^{-6}$ $\Omega$ m, $U_0 = 0.15$ eV-T, $\eta = 2\times10^{-7}$ N s/m$^2$, $\kappa_{p0} = 1.3\times10^4$ N/m$^2$. Physical meaning of the various parameters is explained in the text.

## V. DISCUSSION OF THE RESULTS

In Table II we considered various possible anomalous regimes in terms of the functional form of $R_s(H_{\rm rf})$ and $X_s(H_{\rm rf})$, as well as possible physical mechanisms that might be responsible for the anomalous behavior. The table also contains a list of various microscopic and macroscopic parameters (such as quasiparticle scattering rate $\tau$, superfluid density $n_s$, and flux flow resistivity of weak links $\rho_{fJ}$) and their expected field dependences. As far as the physical mechanisms are concerned, three possible scenarios are considered: the shunted grain weak link model (GSWLM),[18] the magnetic field-induced recovery of superconductivity,[20] and the nonlinear two-fluid model with field-dependent scattering rate.[19] As was recently shown by Velichko and Porch,[18] in a superconductor containing weak links some of which are shunted by another superconducting grain a situation is possible when $R_s$ decreases with magnetic field ($H_{\rm rf}$ or $H_{\rm dc}$), while $X_s(H)$ behaves in the normal way, i.e., grows. A similar scenario is possible within the framework of the modified TFM, in which the scattering time is considered to decrease with increased $H$, as recently suggested by Hein.[19,38] These two models can well account for the first scenario in the table, when only $R_s$ decreases with $H$. However, the other two scenarios in which $X_s(H)$ is decreasing function of $H$ cannot be described within the aforementioned two models. Those types of behavior, to our best understanding, should necessarily involve some sort of recovery of the superfluid density with increased magnetic field. The various physical mechanisms[9,20–29] that may lead to such a recovery effect are mentioned in Sec. I. However, at present we are not aware of any theoretical model of $Z_s(H)$ incorporating those scenarios. Thus, to summarize the results of Table II, we should emphasize that within the most general formulation of the surface impedance (if we admit that quasiparticle scattering is the dominant dissipation mechanism) the scenarios, in which $X_s(H)$ is decreasing function of $H$, or both $X_s(H)$ and $R_s(H)$ decrease, should necessarily consider recovery of the superconducting condensate as the result of increased magnetic field.

As one can see in Fig. 17, at low values of $\Delta X_s/R_c$

TABLE II. Various scenarios and possible mechanisms responsible for the anomalous behavior. Here $B = \mu_0 H$, and $H$ stands for both rf and dc magnetic fields.

| Anomalous scenario | Parameters | Mechanisms |
|---|---|---|
| $R_s(B)\downarrow$, $X_s(B)\uparrow$ | [a]$\tau(B)\downarrow$ | Non-linear TFM [d] [see |
| | $\tau=$const, [b]$n_s(B)\downarrow$, | Refs. 19,38] |
| | [c]$\rho_{Jf}(B)\uparrow$ | GSWLM [e] [see Ref. 18] |
| $R_s(B)\uparrow$, $X_s(B)\downarrow$ | $n_s(B)\uparrow$, and $\tau(B)\uparrow$ strongly | Recovery of the condensate |
| | or $\tau=$const and $\rho_{Jf}(B)\uparrow$ | and reduced scattering [f] |
| | | or enhanced flux flow |
| $R_s(B)\downarrow$, $X_s(B)\downarrow$ | $n_s(B)\uparrow$, and | Recovery of the condensate, |
| | $\tau=$const or $\tau(B)\uparrow$ | flux flow negligible |
| | very weakly | |

[a]Here $B=\mu_0 H$, and $H$ stands for both rf and dc magnetic fields.
[b]Quasiparticle scattering rate.
[c]Cooper pair concentration.
[d]Flux flow resistivity of the weak links.
[e]TFM stands for the two-fluid model.
[f]GSWLM stands for grain shunted weak link model.
[g]This may refer to the mechanism of the field-induced alignment of the magnetic impurity spins (Ref. 20) or any other mechanism having the same effect on $n_S(B)$.

(that in turn correspond to low values of $H_{\rm rf}$) all $\Delta R_s/R_c(\Delta X_s/R_c)$ curves for both samples under various external conditions (such as different $T$ and $H_{\rm dc}$) fall closely to the TFM curves. This is a natural result to expect since at low $H_{\rm rf}$ and zero (or weak) $H_{\rm dc}$, when no magnetic vortices penetrate into the films, quasiparticle scattering must be a dominant dissipation mechanism. Another feature to note is that all the experimental curves have a shape with upward curvature, similar to that of the theoretical TFM curve, whereas the flux motion (CCM) curve has a downward curvature. This is another argument in favor of the quasiparticle scattering being the dominant mechanism of the nonlinear dissipation. However, with increased level of external perturbation (microwave or dc field, e.g.), departure from the TFM scaling towards the CCM behavior becomes apparent (see Fig. 17). This suggests that with enhanced $H$ (dc or microwave) vortices may penetrate into the films (most likely through the weak links) and contribute to the microwave dissipation. Though such effect is relatively small (as can be judged from Fig. 17), it can well account for the uncorrelated behavior of $R_s(H_{\rm rf})$ and $X_s(H_{\rm rf})$ that is typically observed in both samples.

We proceed further by considering the structural differences between the two films. As seen from Table I, films TF1 and TF2 were prepared under quite different deposition conditions (deposition $T$'s were 640 and 690 °C, respectively), that resulted in different microstructure of the films. Film TF1 has a factor of $\sim$1.5 larger average surface roughness (3.5–5 nm versus 2–2.5 nm for TF2), wider rocking curve (1.04° versus 0.55° for TF2), longer $c$ axis (11.757 Å versus 11.699 Å). The first two parameters indicate that film TF1 must have a poorer $ab$-plane orientation and higher granularity that are necessarily related to a higher weak link or defect density compared to TF2. This is also consistent with the lower value of the residual surface resistance $R_{\rm res}$ and the higher penetration depth $\lambda(0)$ for this sample (35 $\mu\Omega$ and 210 nm compared with 50 $\mu\Omega$ and 135 nm for TF2). Since $R_s \sim \sigma_1 \lambda^3$, the combination of lower $R_{\rm res}$ and higher $\lambda$ for film TF1 suggests that $\sigma_1$ for this sample is significantly lower than that for TF2. This in turn means that the product $n_n\tau$ is considerably smaller for TF1 compared to that of TF2 (since $\sigma_1 \sim n_n\tau$). Now, if we recall that sample TF1 has a higher defect density and, therefore, most likely a higher residual density of the unpaired electrons $n_n(0)$, we immediately come to the conclusion that residual scattering time $\tau(0)$ for TF1 is considerably shorter than that for TF2. This, again, is in line with our assumption that film TF1 has a higher density of defects or impurities that play a role of additional scattering centers. Thus having admitted that quasiparticle scattering rate in sample TF2 is lower, we might expect that this dissipation channel will be more ''resistant'' to an additional external perturbation (microwave or dc magnetic field, e.g.), and therefore will saturate at higher levels of the perturbation. This latter assumption is confirmed by Fig. 17 (see the inset), where we can see that the experimental data for TF1 (triangles) depart from the TFM (quasiparticle) scaling much earlier than those for film TF2 (circles).

As found in Sec. III, both microwave and dc magnetic fields can produce anomalous behavior of $Z_s$. However, the effects of $H_{\rm rf}$ and $H_{\rm dc}$ are often rather different (see Figs. 5, 6, 7, 8 and comments to them in the text of Sec. III). For instance, for sample TF1 $H_{\rm rf}$ alone (in the absence of the dc field) always leads to increase in $X_s$, whereas $H_{\rm dc}$ may lead to decrease in $X_s$ even at quite low $H_{\rm rf}$. Such a difference in the effect of the microwave and static fields may suggest two alternative conclusions. First, the operating frequency ($\sim$8 GHz) of our measurements may be pretty close to the scattering rate of the anomalous mechanism or, in other words, the sample could be driven towards the dynamic nonlinear response regime, in which $\omega\tau \sim 1$. And second, $H_{\rm rf}$ and $H_{\rm dc}$ penetrate rather differently into the samples and, therefore, may affect different spatial regions of the films.

TABLE III. Experimental values of the $r=\Delta R_s^{rf}/\Delta X_s^{rf}$ parameter and its dependences on temperature, frequency and magnetic field.

| Samples | $r$ value | $T$ dependence | $f$ dependence | $H_{rf}$ dependence |
|---|---|---|---|---|
| TF1, 8 GHz, 15–20 K [a] | $-0.15<r<0.4$ | ~Independent | Increase | Nonmonotonic |
| TF1, 16 GHz, 15 K [a] | $-0.15<r<0.5$ | Unknown | Increase ($\lesssim$10 kA/m), then ~independent | Independent ($\lesssim$10 kA/m), then decrease |
| TF1, 8 GHz, 15 K, $H_{dc}\geqslant 10$ mT [a] | $0.004<r<0.03$ | Unknown | Increase | Increase |
| TF1, 16 GHz, 15 K, $H_{dc}\geqslant 10$ mT [a] | $0.03<r<0.12$ | Unknown | Increase | Increase |
| TF1, 8 GHz, $\geqslant 20$ K [b] | $0.01<r<0.02$ | Decrease | Nonmonotonic | Nonmonotonic |
| TF1, 16 GHz, $\geqslant 20$ K [b] | $0.03<r<0.12$ | Decrease | ~Independent | Decrease ($\lesssim$0.3 kA/m), then independent |
| TF2, 8 GHz, 40–50 K [a] | $-1.0<r<0.6$ | Nonmonotonic (min at ~45 K) | Unknown | ~Independent |
| TF2, 16 GHz, 40–50 K [a] | Absent | Absent | Absent | Absent |
| TF2, 8 GHz, $<40$ and $>50$ K [b] | $0.1<r<0.5$ | Increase $<40$ K, Independent $>50$ K | ~Independent | ~Independent |
| TF2, 16 GHz, $<40$ and $>50$ K [b] | $0.1<r<1.0$ | Increase $<40$ K, Decrease $>50$ K | ~Independent | ~Indepdent |

[a]Subscript *a* marks the data corresponding to the anomalous regime.
[b]Subscript *b* marks the data corresponding to the normal dissipation regime.

Another interesting effect we would like to mention here is that aging of the films affected their microwave performance, and especially the anomalous behavior. We have found that for film TF2 in about a year of storage after the main measurements reported here were made, not only the frequency scaling of $R_s$ in the linear regime has changed [cf., Figs. 10(b) and 11(b)], but also the anomalies in $Z_s(H_{rf})$ have completely disappeared. This strongly suggests that oxygen content of the film, the parameter that deteriorated from $>6.9$ to 6.78 over the above period, is a possible clue to the anomalous nonlinear behavior. However, at the moment the precise mechanism of how the oxygen content affects the appearance of the microwave anomalies is not understood.

Another important issue is the frequency dependence of the $r$ parameter in the anomalous regime. For sample TF1 in zero dc field the $r$ parameter is seen to slightly increase with $f$ in the anomalous regime ($T\leqslant 20$ K) and virtually independent of $f$ in the normal nonlinear regime [$T\geqslant 20$ K, see Fig. 12]. However, when dc field is applied, the frequency dependence of the $r$ parameter in the anomalous regime is remarkably enhanced (see Fig. 16). This effect is absent at higher $T$ (not shown in the figure) in the normal nonlinear regime, where the application of the dc field does not noticeably affect the frequency dependence of $r$ ($r$ strongly increases with $f$ in both zero and finite dc magnetic field). Thus, for sample TF1 there seem to exist two different mechanisms of the nonlinear anomalous response: the first, in zero dc fields, when only $R_s(H_{rf})$ exhibits decrease, the $r$ parameter is weakly frequency dependent, and its modulus takes on values between 0.1–1; and the second, in finite dc fields, when both $R_s(H_{rf})$ and $X_s(H_{rf})$ decrease in correlated manner, $r$ parameter strongly increases with $f$ and takes on values between 0.001–0.1. Similarly to TF1, for film TF2 the $r$ parameter is seen to increase with frequency in the anomalous $T$ range ($40<T<50$ K) (see Fig. 13) with typical values of $r$ being ~0.1 and ~1 at 8 and 16 GHz, respectively. Outside this $T$-range $r$ parameter is nearly frequency independent. Unfortunately, we do not have dc field measurements on this sample at 40 K, where the strongest anomaly in $X_s(H_{rf})$ has been observed and, therefore, cannot comment on how dc field would affect that anomaly. Here, at other temperatures (such as 15 and 60 K), at which anomalies are only seen in a trapped magnetic flux (see Figs. 7 and 8), the effect of $H_{dc}$ on $H_{rf}$ dependence and values of $r$ is quite negligible. The exception is the case of $H_{dc}$ of 5 mT at 60 K, that is seen to drive $r$ parameter towards large ($\sim -1$) negative values (see Fig. 15). Under these conditions an anomaly in $X_s(H_{rf})$ is also observed (see Figs. 7).

Table III summarizes $T$, $f$, and $H_{rf}$ dependences as well as typical values of the $r$ parameter for the two films studied in this work. The results are presented for both the anomalous and normal nonlinear regimes. In addition, the theoretical $r$ values together with its $T$, $f$, and $H_{rf}$ dependences predicted by TFM and CCM are given in Table IV. By comparing the two tables, one can see that in some cases rather good matches between the theory and experiment are seen in terms of $r(T,f,H)$ and $r$ values. For film TF1, for instance, the regime of the correlated anomalies in $R_s(H_{rf})$ and $X_s(H_{rf})$, which is observed at 15 K in a frozen dc flux, matches well the predictions of the TFM (with the Ginzburg-Landau pair breaking as the responsible nonlinear mechanism) in terms of $r$ values and $r(f,H_{rf})$. On the other hand, it also overlaps with the predictions of the CCM in terms of $r(H_{rf})$. In other cases of the anomalous behavior it is more difficult or even impossible to draw any conclusions because of either a lack of the experimental data (such as frequency dependence of

TABLE IV. Theoretical values of the $r=\Delta R_s^{\mathrm{rf}}/\Delta X_s^{\mathrm{rf}}$ parameter and its dependences on temperature, frequency, and magnetic field.

| Theory | $r$ value | $T$ dependence | $f$ dependence | $H$ dependence [a] |
|---|---|---|---|---|
| Flux creep (CCM), low field | $0.1<r<1.0$ (1 mT$<B<$50 mT) | Increase at low $B$ Nonmonotonic (max) at $B\geqslant 10$ mT | Increase at low $B$ Nonmonotonic (max) at $B\geqslant 10$ mT | Increase |
| Flux flow (CCM), low field | $1.0<r<7.0$ (1 mT$<B<$50 mT) | Increase at low $B$ Nonmonotonic (max) at $B\geqslant 10$ mT | Increase at low $B$ Nonmonotonic (max) at $B\geqslant 10$ mT | Increase |
| GL depairing (TFM), low field | $0.04<r<0.1$ (1 mT$<B<$50 mT) | Nonmonotonic min at $t\sim 0.7$ | Increase | Independent at low $B$ Increase at $B\geqslant 10$ mT |

[a]Here $B=\mu_0 H$, and $H$ stands for both rf and dc magnetic fields.

$R_s$ in the anomalous regime for film TF2, e.g.) or inapplicability of the models in their classical formulation to the available experimental data (such as, e.g., negative $r$ values for TF1 at 15 K and 0 mT). All this suggests that at the moment due to the lack of experimental data (such as $T$ and $f$ dependences of $r$ in the anomalous regime, e.g.) and similarity in the models' predictions for $r(H)$ we are not able to unambiguously distinguish between the two mechanisms in terms of $r(T,f,H)$. However, in terms of $r$ values most of the experimental data (especially those corresponding to the anomalous behavior) presented in Table III clearly stand apart from the vortex motion mechanisms described by the CCM. This is obviously in line with the results of Fig. 17. In addition we can see that despite the deviation of $\Delta R_s/R_c(\Delta X_s/R_c)$ curves from TFM scaling and departure towards CCM scaling with increased $H_{\mathrm{rf}}$, the shape of the experimental curves is clearly reminiscent of that of the TFM curves, and is quite dislike the shape of the CCM curve. All this strongly suggests that even though the vortices are inevitably present in the films upon field cooling, they do not noticeably contribute to the nonlinear microwave dissipation, and the flux motion mechanisms are believed to remain of minor importance for all the experiments reported in this work.

## VI. CONCLUSION

Two high-quality epitaxial YBaCuO thin films on MgO substrates have been investigated for temperature $T$, frequency $f$, static $H_{\mathrm{dc}}$ and microwave $H_{\mathrm{rf}}$ magnetic field dependences of the surface impedance $Z_s=R_s+jX_s$ using the coplanar resonator technique at 8 and 16 GHz. A dc magnetic field up to 12 mT was applied perpendicularly to the film surface in the field cooled regime. At certain temperatures, both films exhibit anomalies in $H_{\mathrm{rf}}$ dependences of either the surface resistance $R_s$ or surface reactance $X_s$. Here, the qualitative behaviors of $R_s(H_{\mathrm{rf}})$ and $X_s(H_{\mathrm{rf}})$ are generally not correlated (in sense that one may decrease, whereas the other increases). In zero dc field film TF1 exhibits anomaly only in $R_s(H_{\mathrm{rf}})$ and only at low $T$ (15 K), whereas film TF2 mainly shows anomalies in $X_s(H_{\mathrm{rf}})$ and only at intermediate temperatures (40–50 K).

Measurements in the field cooled state showed that the trapped magnetic flux may produce a dramatic effect on $Z_s(H_{\mathrm{rf}})$, especially on $X_s(H_{\mathrm{rf}})$. For instance, the dc field as low as 5 mT may completely invert the $H_{\mathrm{rf}}$ dependence of $X_s$, turning it from increasing to decreasing function of $H_{\mathrm{rf}}$. The impedance plane analysis revealed that such a change is accompanied by an abrupt change in the value and $H_{\mathrm{rf}}$ and $f$ dependences of the $r$ parameter and is, therefore, associated with a change in the nonlinear mechanism.

We performed a detailed impedance plane analysis of the data involving consideration of $T$ and $H_{\mathrm{rf}}$ dependences of the differential loss tangent $\tilde{r}=\partial R_s/\partial X_s$, and comparing them with those expected from the two-fluid model (TFM) and Coffey-Clem model (CCM) for vortex motion. The analysis revealed that for $H_{\mathrm{rf}}\lesssim 10$ kA/m the dissipation mechanism is due to the nonlinear dynamics of quasiparticles (Ginzburg-Landau pair breaking), whereas at higher $H_{\mathrm{rf}}$ a clear departure from the TFM scaling towards the vortex motion mechanisms is observed. Here, even in this higher field range $\Delta R_s/R_c(\Delta X_s/R_c)$ curves and their functional form in the anomalous regime tend to be much closer to the TFM scaling curve, rather than to the CCM limit. All this suggests that the vortex motion brings relatively slight modification to the nonlinear mechanism, which is mainly governed by the dynamics of quasiparticles. In addition, a simple qualitative analysis within the standard TFM has shown that (provided that quasiparticle scattering is a dominant dissipation mechanism) correlated decrease of $R_s(H_{\mathrm{rf}})$ and $X_s(H_{\mathrm{rf}})$, or just decrease in $X_s(H_{\mathrm{rf}})$ alone should necessarily involve some sort of recovery of the superconducting condensate with increased magnetic field (rf or dc).

It was also found that aging of film TF2 not only led to a change in the frequency dependence of $R_s$ in the linear regime (the scaling exponent, $n$ has changed from $\sim 1.7$ to 2 after a year of storage), but also to complete disappearance of the anomalous effects in $Z_s(H_{\mathrm{rf}})$. X-ray measurements on that sample revealed that the film lost significant amount of oxygen ($\delta\simeq 6.78$ compared to $\delta\gtrsim 6.9$ in the freshly grown film). This leads us to a conclusion that the oxygen content of YBaCuO films plays an unknown but very important role in the occurrence of the microwave anomalies discussed in this paper. Proper understanding of the role of oxygen dop-

ing in this phenomenon, as well as revealing precise physical mechanism(s) (which, as was shown here, are most likely related to the quasiparticle dynamics) of the anomalous nonlinear microwave response of YBaCuO films present very challenging tasks to be solved by the researchers in the near future.

**ACKNOWLEDGMENTS**

We are grateful to Dr. Tim Jackson for fruitful discussion and valuable comments on the paper and to Professor R. G. Humphreys for kindly providing us with the samples for this research. This work was supported by EPSRC Grant No. GR/L65581/01.

[1] M. J. Lancaster, *Passive Microwave Device Application of High-Temperature Superconductors* (Cambridge University Press, Cambridge, 1997), and references therein.

[2] M. A. Hein, *High-Temperature Superconductor Thin Films at Microwave Frequencies* (Springer, Berlin, 1999), and references therein.

[3] A. M. Portis, *Electrodynamics of High-Temperature Superconductors* (World Scientific, Singapore, 1992).

[4] J. Halbritter, J. Appl. Phys. **68**, 6315 (1990), and references therein.

[5] P. P. Nguyen, D. E. Oates, G. Dresselhaus, and M. S. Dresselhaus, Phys. Rev. B **48**, 6400 (1993); P. P. Nguyen, D. E. Oates, G. Dresselhaus, M. S. Dresselhaus, and A. C. Anderson, *ibid.* **51**, 6686 (1995).

[6] M. A. Golosovsky, H. J. Snortland, and M. R. Beasley, Phys. Rev. B **51**, 6462 (1995).

[7] J. Halbritter, J. Supercond. **8**, 690 (1995); **10**, 91 (1997).

[8] D. P. Choudhury, B. A. Willemsen, J. S. Derov, and S. Sridhar, IEEE Trans. Appl. Supercond. **7**, 1260 (1997).

[9] M. A. Hein, C. Bauer, W. Diete, S. Hensen, T. Kaiser, V. Z. Krezin, and G. Mueller, J. Supercond. **10**, 485 (1997).

[10] A. P. Kharel, A. V. Velichko, J. R. Powell, A. Porch, M. J. Lancaster, and R. G. Humphreys, Phys. Rev. B **58**, 11 189 (1998).

[11] B. B. Jin, X. S. Rao, C. Y. Tan, and C. K. Ong, Physica C **316**, 224 (1999); X. S. Rao, C. K. Ong, B. B. Jin, C. Y. Tan, S. Y. Xu, P. Chen, J. Li, and Y. P. Feng, *ibid.* **328**, 60 (1999).

[12] M. Spiewak, Phys. Rev. **113**, 1479 (1959).

[13] J. D. Thompson, M. P. Maley, and J. R. Clem, J. Appl. Phys. **50**, 3531 (1979).

[14] J. R. Clem, J. Appl. Phys. **50**, 3518 (1979).

[15] g. M. Eliashberg, Pis'ma Zh. Éksp. Teor. Fiz. **11**, 186 (1970) [JETP Lett. **11**, 114 (1970)].

[16] A. Kharel, K. H. Soon, J. R. Powell, A. Porch, M. J. Lancaster, A. V. Velichko, and R. G. Humphreys, IEEE Trans. Appl. Supercond. **9**, 2121 (1999).

[17] A. V. Velichko, A. Porch, M. J. Lancaster, and R. G. Humphreys, IEEE Trans. Appl. Supercond. **11** Pt.3, 3497 (2001).

[18] A. V. Velichko and A. Porch, Phys. Rev. B **63**, 094512 (2001).

[19] M. A. Hein (private communication).

[20] Yu. N. Ovchinnikov and V. Z. Kresin, Phys. Rev. B **54**, 1251 (1996), and references therein.

[21] V. Z. Kresin, S. A. Wolf, and Yu. N. Ovchinnikov, Phys. Rev. B **53**, 11 831 (1996).

[22] M. A. Hein, T. Kaiser, and G. Mueller, Phys. Rev. B **61**, 640 (2000).

[23] L. Alff, A. Beck, R. Gross, A. Marx, S. Kleefisch, T. Bauch, H. Sato, M. Naito, and G. Koren, Phys. Rev. B **58**, 11 197 (1998); S. Sinha and K.-W. Ng, Phys. Rev. Lett. **80**, 1296 (1998).

[24] J. Voit, Rep. Prog. Phys. **57**, 977 (1994).

[25] M. Ogata and P. W. Anderson, Phys. Rev. Lett. **70**, 3087 (1993).

[26] H. L. Edwards, D. J. Derro, A. L. Barr, J. T. Markert, and A. L. de Lozanne, Phys. Rev. Lett. **75**, 1387 (1995).

[27] C. Howald, P. Fournier, and A. Kapitulnik, cond-mat/0101251 (unpublished).

[28] R. S. Markiewicz and C. Kusko, cond-mat/0102438 (unpublished).

[29] C. Kusko, Z. Zhai, R. S. Markiewicz, and S. Sridhar, cond-mat/0102288 (unpublished).

[30] M. A. Hein, P. Hirst, R. G Humphreys, D. E. Oates, and A. V. Velichko, Appl. Phys. Lett. **80**, 1007 (2002).

[31] X. S. Rao, C. K. Ong, and Y. P. Feng, Appl. Phys. Lett. **77**, 2897 (2000).

[32] M. W. Coffey and J. R. Clem, Phys. Rev. Lett. **67**, 386 (1991); J. R. Clem and M. W. Coffey, J. Supercond. **5**, 313 (1992).

[33] At the moment of taking the microwave measurements presented in Sec. III both films were about 3 years old.

[34] A. Porch, M. J. Lancaster, and R. G. Humphreys, IEEE Trans. Microwave Theory Tech. **43**, 306 (1995).

[35] A. Reznik, IEEE Trans. Appl. Supercond. **7**, 1474 (1997).

[36] Film TF2 was cleaved into two slabs shortly after the film fabrication. The part of the film on which the majority of the measurements reported in this paper were made is referred to as ''film TF2,'' whereas the other part is referred to as the ''reference part.''

[37] Here we should note that in the x-ray measurements oxygen content is determined from the *c*-axis length. Though this relationship is not always unambiguous and may be influenced by other characteristics of the films (such as cation disorder, e.g.), in general for the films prepared by the same deposition method a longer *c* axis usually corresponds to the reduced oxygen content.

[38] M. A. Hein, P. Hirst, R. G Humphreys, D. E. Oates, and A. V. Velichko, cond-mat/0105613 (unpublished).

[39] T. Hylton, A. Kapitulnik, M. R. Beasley, J. P. Carini, L. Drabek, and G. Gruner, Appl. Phys. Lett. **53**, 1343 (1988); C. Attanasio, L. Maritato, and R. Vaglio, Phys. Rev. B **43**, 6128 (1991).

[40] J. R. Powell, A. Porch, A. P. Kharel, M. J. Lancaster, R. G. Humphreys, F. Wellhofer, and C. E. Gough, J. Appl. Phys. **86**, 2137 (1999).

[41] M. Mahel, *Studies of High-Temperature Superconductors*, edited by A. Narlikar (Nova, New York, 1996), Vol. 17, p. 30.